Metal-Shell Effect on Multimode Antennas for Wideband Mobile Applications

Kaifeng Li, Wendi Yan, *Graduate Student Member, IEEE*, Yongjian Zhang, *Member, IEEE*, Peihang Li, Pengyu Fu, Yixiang Song, Hui Lin, Heng Guo, Shumin Liao, and Yue Li, *Senior Member, IEEE*

***Abstract*—The metal shell is usually considered as a negative factor that degrades the impedance bandwidth of mobile terminal antennas. Here, we propose a different perspective on utilizing the metal shell to enhance the bandwidth. Through our study, beyond the antenna's own modes, the cavity modes induced between the metal shell and the motherboard are also excited. By designing the antenna and the metal shell jointly, multiple cavity modes are controlled to enhance the bandwidth. As an example, a segmented half-loop antenna is designed in a tablet computer to demonstrate the positive effect of the metal shell on antenna's bandwidth. The experimental results indicate that a −6-dB impedance bandwidth of 3.27–8.46 GHz is achieved with a compact antenna dimension of $0.28 \times 0.047 \times 0.011\ \lambda_L^3$, exhibiting the potentials for antenna designs in various metal-shell mobile terminals.**

***Index Terms*—Metal shell, mobile antennas, mu-near-zero (MNZ) antennas, multiple-frequency antennas, wideband antennas.**

I. Introduction

With the rapid advancement of wireless systems, mobile terminals have undergone multiple iterations. In modern mobile terminals, metal-shell architectures are widely used due to their high structural strength, excellent heat dissipation, and sleek appearance. These features are particularly beneficial for high-performance devices such as tablet computers and laptops [1], [2], [3], [4]. Meanwhile, the widespread adoption of multiple new communication technologies, such as wireless fidelity (Wi-Fi), fifth generation (5G), and ultrawideband (UWB), has made wideband antennas an essential component of wireless systems [5], [6], [7], [8], [9], [10]. However, the presence of the metal shell introduces significant challenges for antenna design. On the one hand, it obstructs electromagnetic radiation over a large area [11], [12]. On the other hand, it introduces substantial parasitic distributed capacitance and inductance, which deteriorate the impedance matching [13], [14], [15], [16]. Consequently, it is a significant challenge to design wideband antennas for metal-shell mobile terminals.

In recent years, considerable research has focused on antenna design in metal-shell terminals [17], [18], [19], [20], [21], [22], [23], [24], [25], [26], [27], [28], [29]. Among these designs, multimode antennas are particularly favored for their potential to achieve wideband or multiband performance, and three main approaches emerge to mitigate the negative impact of the metal shell. The first approach involves using additional circuit networks [17], [18], [19], [20], [21]. Through specific matching circuit design, the antennas in [17], [18], and [19] achieve improved matching within several limited bands. Moreover, reconfigurable circuits are employed in [20] and [21] to dynamically cover multiple bands. The second approach employs balanced antenna structures [22], [23]. The antenna in [22] reduces the influence of metal-shell currents using a balanced segmented loop design, though its bandwidth remains constrained by the antenna's physical dimensions. The third approach involves modifying the metal-shell structure [24], [25], [26], [27], [28], [29]. By etching notches or slots onto the metal frame and back cover, the antenna can radiate through slot currents without interference from the metal shell. For example, the antenna in [26] achieves a wide bandwidth of 57% through a simple open-slot antenna with a microstrip feeding, while this approach compromises the integrity of the metal shell, limiting its application in engineering. In general, all these methods indicate that the metal shell degrades the antenna matching and aim to minimize its impact as much as possible.

In this article, we propose an approach for enhancing the bandwidth of multimode antennas by leveraging cavity modes induced between the metal shell and the motherboard, which enables the metal shell to contribute positively to broadband impedance matching. Specifically, we introduce a segmented half-loop antenna, which is equivalent to a mu-near-zero (MNZ) antenna [30], [31], [32], [33], [34], [35]. Owing to its multimode synergy capability, several excited loop modes simultaneously couple and excite multiple cavity modes. Through the joint design of the antenna and the metal shell, the bandwidth is obviously expanded. With dimensions of $0.28 \times 0.047 \times 0.011\ \lambda_L^3$ (λ_L is the free-space wavelength at the lowest frequency of operating band), the half loop is symmetrically replicated in a tablet computer for

Received 13 June 2025; accepted 24 July 2025. Date of publication 7 August 2025; date of current version 30 October 2025. This work was supported in part by the National Key Research and Development Program of China under Grant 2021YFA0716601, in part by the National Natural Science Foundation of China under Grant U22B2016, and in part by Lenovo. *(Corresponding author: Yue Li.)*

Kaifeng Li, Wendi Yan, Yongjian Zhang, Peihang Li, and Pengyu Fu are with the Department of Electronic Engineering, Tsinghua University, Beijing 100084, China.

Yixiang Song, Hui Lin, Heng Guo, and Shumin Liao are with Tablet Business, Lenovo, Beijing 100193, China.

Yue Li is with the Department of Electronic Engineering, Beijing National Research Center for Information Science and Technology, State Key Laboratory of Space Network and Communications, Tsinghua University, Beijing 100084, China (e-mail: lyee@tsinghua.edu.cn).

Digital Object Identifier 10.1109/TAP.2025.3594883

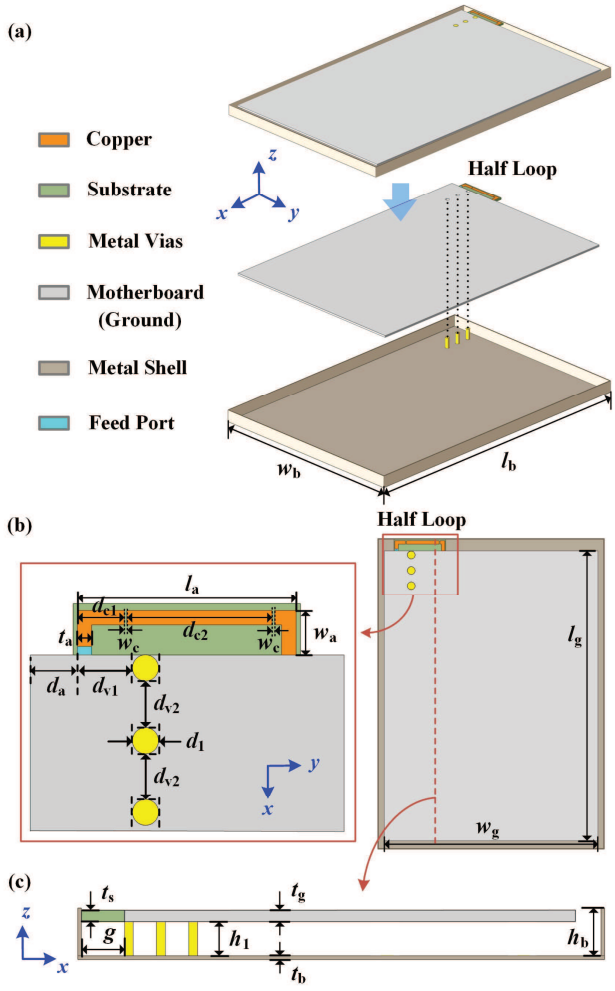

Fig. 1. Geometry configuration of the half-loop antenna in a mock-up metal-shell tablet computer. (a) Exploded view. (b) Top view. (c) Side view.

multiple-input–multiple-output (MIMO) applications, and two metal vias are used to improve the isolation. The measured results validate the simulated ones, confirming the wideband coverage from 3.27 to 8.46 GHz. These results demonstrate the effectiveness of the metal shell in extending the bandwidth of the mobile terminal antennas, revealing its potential for antenna designs in metal-shell mobile terminals.

II. Antenna Configuration and Evolution

Fig. 1 illustrates the configuration of the proposed antenna and its operational environment in the mock-up tablet computer. It is noteworthy that the structure of most commercial tablet computers, which feature a metal-shell environment, is usually quite complex and intricate, posing challenges to antenna optimization and theoretical analysis. To address this, we simplified the tablet structure by extracting and retaining components that significantly influence the antenna radiation, thereby constructing a simplified mock-up environment for the metal-shell tablet computers. As depicted in Fig. 1(a) and (c), the mock-up comprises two primary components: a metal shell and a motherboard. The metal shell has dimensions $l_b \times w_b \times h_b$ with a thickness of t_b. The motherboard, with a thickness of t_g, is supported above the metal shell at height h_1 using three metal vias, which act as the shorting points for the tablet computer. These metal vias have a diameter of d_1 and are arranged in a row with spacing d_{v2}. The proposed half-loop antenna is placed in the clearance of the tablet computer, as shown in Fig. 1(b). Specifically, the segmented half loop has dimensions of $l_a \times w_a$ and is printed on an F4B substrate ($\varepsilon_r = 2.65$ and $\tan\delta = 0.002$) of thickness t_s. Two gaps are etched into the half loop to serve as distributed capacitances, each with a width w_c and spaced d_{c2} apart. Additionally, the metal vias arranged in a column at the corner are spaced d_{v1} from the antenna port. The proposed antenna is numerically simulated using the commercial simulation software HFSS 2023 R1. The final parameter values are listed in Table I following simulated optimization.

TABLE I
Dimensions of the Proposed Design (Unit: mm)

l_b	w_b	l_a	w_a	t_a	w_c	d_{c1}
206.2	129.2	25.7	4.3	1.7	0.2	6
d_{c2}	d_a	d_{v1}	d_{v2}	d_1	l_g	w_g
16.25	5.5	7.5	5.5	3	196	122
t_s	t_g	t_b	h_b	h_1	g	
1	1	0.6	6.5	5	5	

To facilitate the analysis of the operating principle, Fig. 2 illustrates the evolution process of the proposed antenna, emphasizing the metal-shell effect on multimode antenna design. As shown in Fig. 2(a), Ant. A is a segmented half loop connected to the motherboard, demonstrating its multimode performance in a nonmetal-shell environment. This antenna works in several resonant modes but fails to cover the desired communication bands. To enhance the bandwidth, Ant. B introduces a metal shell behind the motherboard, realizing the high-frequency band but still not completing the coverage of low-frequency band, as illustrated in Fig. 2(b). Furthermore, Ant. C in Fig. 2(c) incorporates a metal shorting block between the metal shell and the motherboard, which provides a shunt inductance to improve the low-frequency impedance matching. Finally, to meet practical engineering requirements, Ant. D replaces the metal block with three metal vias while maintaining the wide bandwidth from 3.2 to 8.6 GHz, as depicted in Fig. 2(d). Next, Sections II-A–II-C provide a detailed analysis of the evolution process, illustrating the principles for bandwidth extension using the metal shell.

A. Ant. A: Half-Loop Antenna Design

The design strategy of Ant. A is illustrated in Fig. 3. Ant. A consists of a segmented half loop and a large motherboard. According to the image theorem and continuity of current, this structure can be regarded as a complete loop, which enables the application of similar design principles as a conventional MNZ loop antenna [22] and thereby supports the analysis of Ant. A as an MNZ half-loop structure, as shown in Fig. 3(a). As depicted in Fig. 3(c), two distributed capacitances are loaded onto the half loop to directly adjust the antenna's effective permeability, enabling the simultaneous excitation of

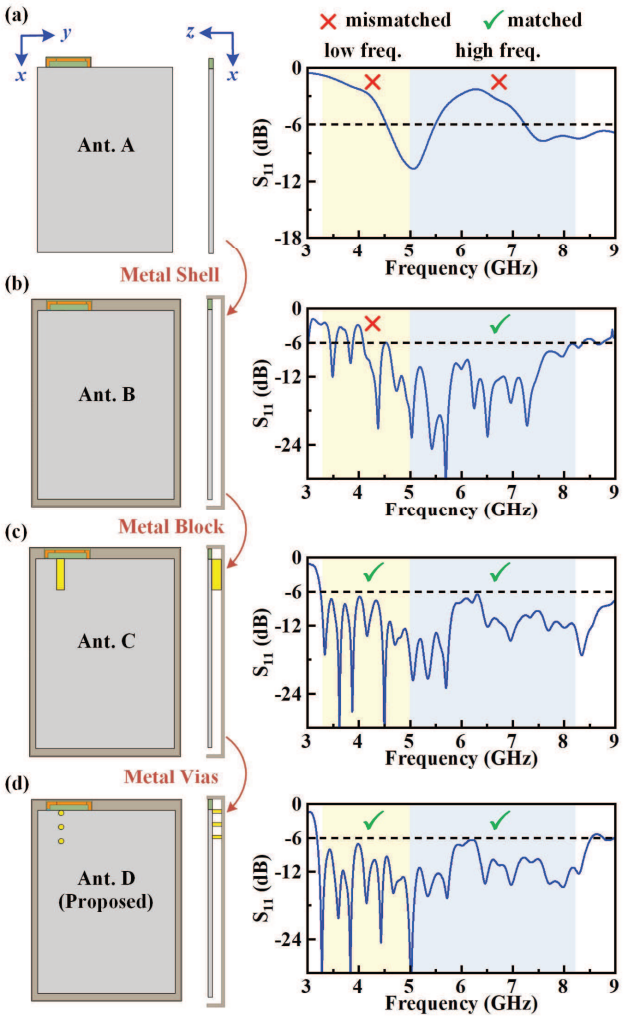

Fig. 2. Evolution process of the proposed antenna element and the corresponding reflection coefficients. (a) Ant. A: single half loop. (b) Ant. B: add a metal shell. (c) Ant. C: add a metal block. (d) Ant. D: replace the metal block with three metal vias.

three loop modes. Similar to the MNZ loop antenna, these modes of MNZ half loop can also be denoted as loop-n^{th}, where n represents the number of current phase reversals on both the half loop and the ground (motherboard). Fig. 3(b) illustrates the surface current distributions for these modes. The fundamental mode, or loop-0$^{\text{th}}$ mode, forms a current loop without any current nulls between the half loop and the metal motherboard, exhibiting quasi-uniform amplitude and phase. At higher frequencies, two high-order modes are excited: the loop-1$^{\text{st}}$ mode, characterized by one current phase reversal on both the half loop and the ground, and the loop-2$^{\text{nd}}$ mode, characterized by two current phase reversals. Compared to a conventional MNZ loop, the MNZ half-loop antenna design achieves similar performance while reducing the antenna size by nearly half, making it well-suited for small clearances in tablet computers. However, due to its limited radiation aperture and constrained multimode synergy capabilities, the MNZ half-loop antenna struggles to meet the wideband requirements of modern mobile terminals.

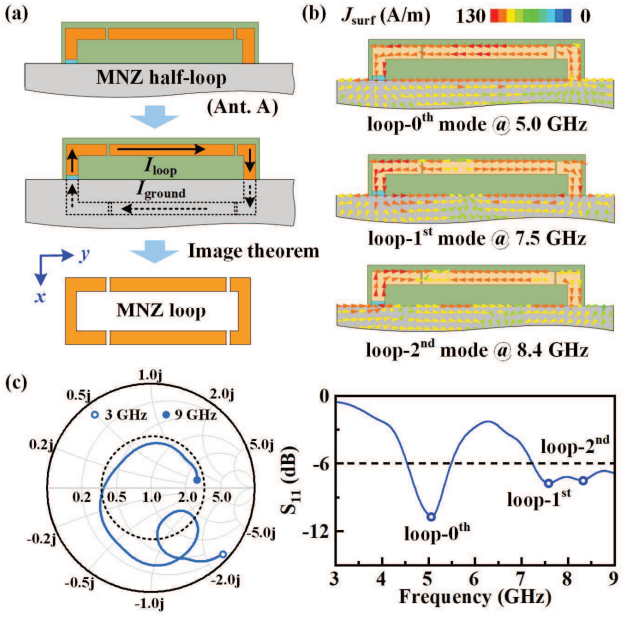

Fig. 3. Half-loop design. (a) Analysis of the image theorem for Ant. A. (b) Simulated surface current distributions of Ant. A at three resonant frequencies. (c) Simulated Smith chart and reflection coefficient of Ant. A.

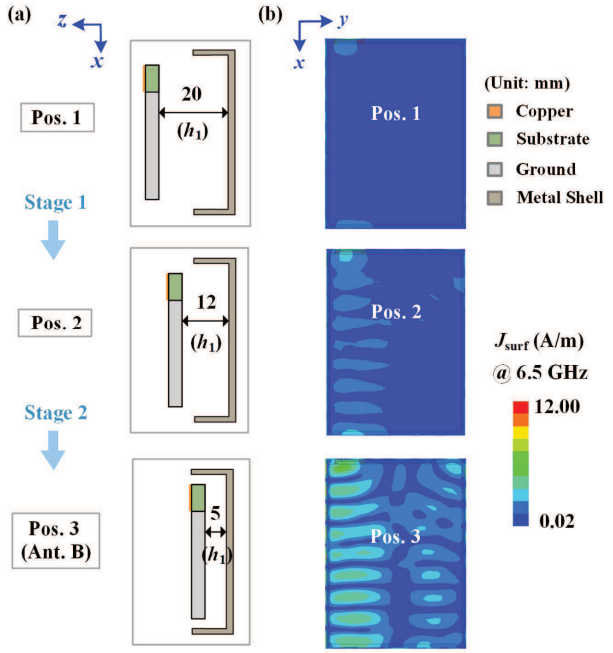

Fig. 4. (a) Evolution of Ant. B. (b) Simulated surface current distributions on the metal shell at different positions.

B. Ant. A to Ant. B: Metal-Shell Effect on Matching

As previously mentioned, the metal shell plays a critical role in bandwidth enhancement. To clarify the specific operating mechanism, the evolution from Ant. A to Ant. B is analyzed, focusing on the effect of varying the distance h_1 between the motherboard and the metal shell. As shown in Fig. 4, when the metal shell is sufficiently distant from the motherboard, the surface currents on the metal shell are negligible. Therefore,

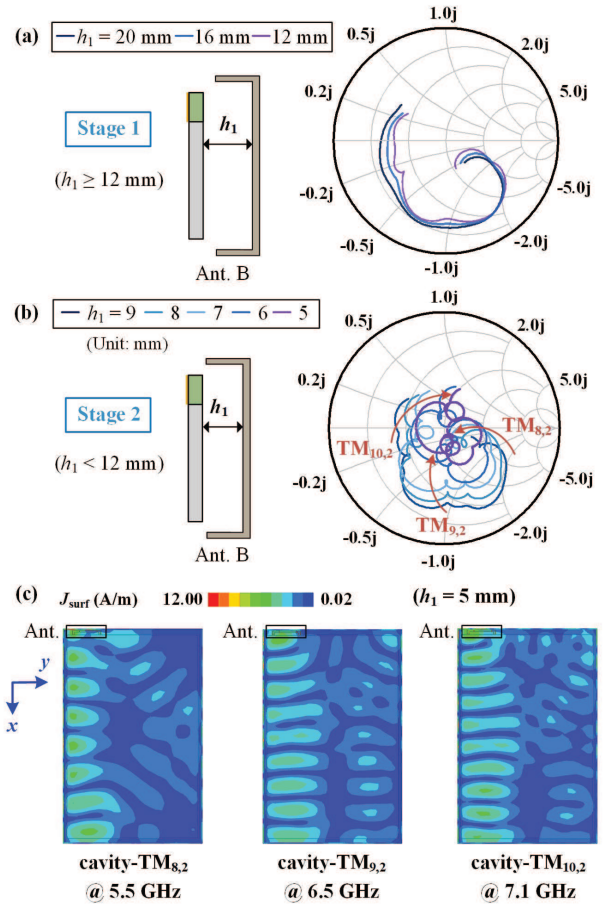

Fig. 5. Analysis of Ant. B. Smith Chart curves with different values of h_1 at 5.1–7.6 GHz when (a) h_1 is larger than 12 mm and (b) h_1 is lower than 12 mm. (c) Simulated surface current distributions on the metal shell of Ant. B at different cavity modes (h_1 = 5 mm).

the metal shell has a minimal impact on antenna performance, which remains almost identical to that of Ant. A. As the metal shell moves closer to the motherboard, the changes in antenna performance can be divided into two stages. In Stage 1 ($h_1 \geq 12$ mm), since the metal shell is still relatively far from the motherboard, weak induced currents are generated on the shell. At this point, the metal shell can be considered a distributed parasitic structure, which affects the antenna's impedance matching. In Stage 2 ($h_1 < 12$ mm), as the metal shell moves closer, stronger induced currents develop on its surface. At this point, a cavity is formed between the metal shell and the motherboard, leading to the coupled excitation of multiple cavity modes. This excitation enhances the antenna's main radiation mode and significantly broadens its bandwidth. A detailed analysis of these two stages is provided next, illustrating the principles behind bandwidth expansion.

Fig. 5(a) illustrates the effect of the metal shell in Stage 1 where $h_1 \geq 12$ mm. Similar to a parallel-plate capacitor, the metal shell and the motherboard can be equivalently modeled as a parasitic distributed capacitance. As shown in the Smith chart, as the distance h_1 decreases, the equivalent capacitance increases. This trend results in an upward rotation of the low-frequency curve, indicating a series capacitance, while the high-frequency curve rotates downward, indicating

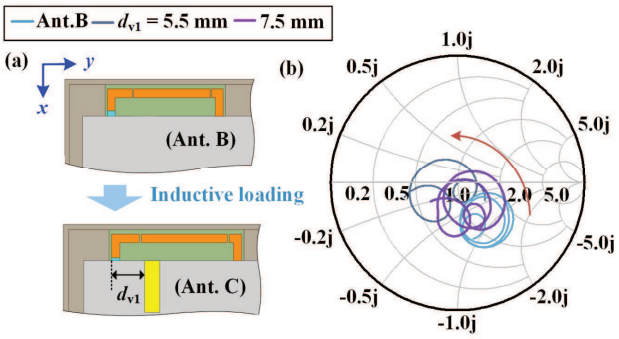

Fig. 6. (a) Evolution from Ant. B to Ant. C. (b) Changes in the Smith chart during the evolution process at 3.3–4.3 GHz.

a shunt capacitance. Since the metal shell remains relatively far from the motherboard in this stage, the effect on impedance matching is quite minor. Fig. 5(b) shows the metal-shell effect on antenna bandwidth in Stage 2 where $h_1 < 12$ mm. As depicted in the Smith chart, with the decrease in h_1, the cavity modes between the metal shell and the motherboard are excited, leading to a significant improvement in antenna's impedance matching. Three main cavity modes, named cavity-$TM_{8,2}$, $TM_{9,2}$, and $TM_{10,2}$, are excited, with their current distributions on the metal shell being depicted in Fig. 5(c). Specifically, the cavity-$TM_{8,2}$ mode at 5.5 GHz has an eight-half-wavelength current distribution along the x-axis and a double-half-wavelength current distribution along the y-axis. Similarly, the cavity-$TM_{9,2}$ mode at 6.5 GHz exhibits a nine-half-wavelength current distribution along the x-axis, while the cavity-$TM_{10,2}$ mode at 7.1 GHz shows a ten-half-wavelength current distribution. Unlike previous approaches, this method incorporates the metal shell as an additional design freedom. By jointly optimizing the antenna and the metal shell while fully utilizing the cavity modes, the high-frequency bandwidth can be enhanced.

C. Ant. B to Ant. C/D: Inductive Loading for Matching

In practical tablet devices, a set of metal structures is typically required to connect the metal shell to the motherboard. This structure can further extend the antenna's low-frequency bandwidth. As shown in Fig. 6(a), a metal cuboid block serving as the shorting structure is added to Ant. B to form Ant. C. Approximately, the metal shell and the motherboard behave as a two-conductor transmission line, and the metal block acts as a short-circuit point. According to the transmission line theory, the feeding port is loaded with an impedance valued

$$Z_L = jZ_C \tan(\beta d_{v1}) \tag{1}$$

where Z_C represents the characteristic impedance of the transmission line, β is the wavenumber, and d_{v1} is the distance between the metal block and the feeding port. When $d_{v1} < \lambda/4$, Z_L indicates a shunt inductance. Fig. 6(b) illustrates the variation in the Smith chart curve of the antenna at 3.3–4.3 GHz. As shown, after introducing the metal block, the impedance curve of Ant. B on the Smith chart rotates upward, resulting in the well-matched curve of Ant. C. Furthermore, by

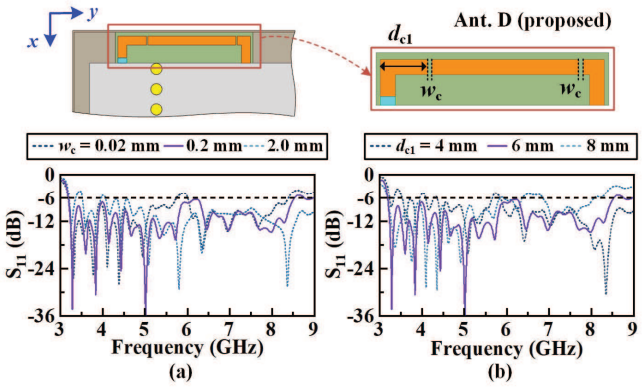

Fig. 7. Simulated reflection coefficient curves for different parameters of Ant. D. (a) w_c. (b) d_{c1}.

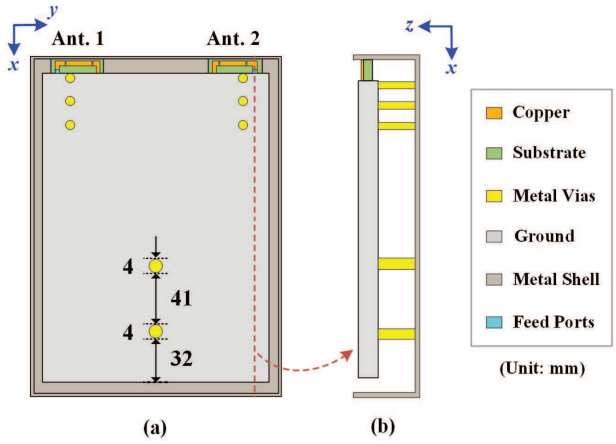

Fig. 8. Geometry configuration of the two-element MIMO antenna in the mock-up metal-shell tablet computer. (a) Top view. (b) Side view.

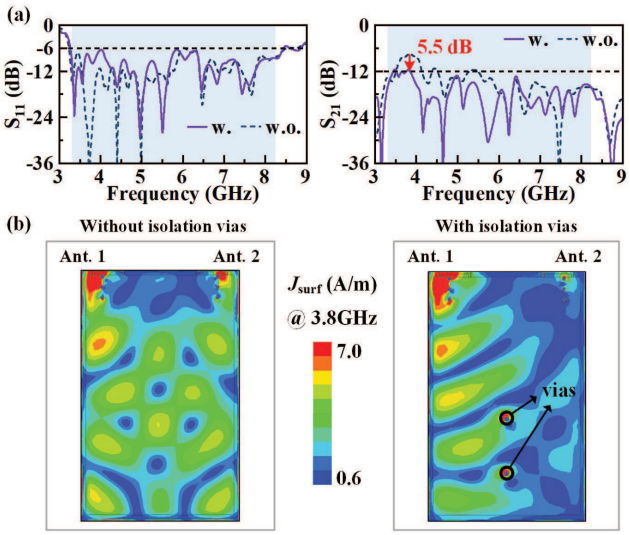

Fig. 9. Comparison of the proposed MIMO antenna with and without the isolation vias. (a) S-parameters. (b) Simulated surface current distributions on the metal shell (only Ant. 1 is excited). (w.: with and w.o.: without.)

adjusting the metal block position d_{v1}, the value of the shunt inductance Z_L can be controlled to enhance the low-frequency bandwidth without additional matching circuits.

Although the design in Ant. C improves the low-frequency matching, the metal block structure is not suitable for practical engineering. Therefore, Ant. D replaces the metal block with three metal vias to meet practical requirements, as shown in Fig. 7. By optimizing the positions and dimensions of the metal vias, Ant. D achieves the same bandwidth as Ant. C. At the same time, the MNZ half-loop antenna, which excites the cavity modes, also plays a crucial role in impedance matching. Specifically, the width w_c of the two gaps etched into the half loop directly determines the distributed capacitance, which affects the effective permeability and further influences the input impedance of the half loop, as shown in Fig. 7(a). Moreover, the distributed capacitance is also influenced by the current magnitude, which in turn depends on the positions of the gaps. As an example, Fig. 7(b) illustrates the effect of the left-side gap position on impedance matching and provides the optimal parameter values. Therefore, compared to traditional loop antennas, the proposed MNZ half-loop antenna offers a significant advantage in effectively adjusting the input impedance. This makes it well-suited for exciting cavity modes in a metal-shell environment for broadband performance.

D. MIMO Antenna Design

To further meet the requirements of MIMO applications, two identical antenna elements are symmetrically positioned in the clearance of the tablet computer, forming a two-element MIMO antenna, as illustrated in Fig. 8. The specific dimensions remain consistent with those listed in Table I, except for d_{v1} set to 6.5 mm for better impedance matching. However, due to the symmetry of the cavity modes, when Ant. 1 is excited, significant mutual coupling occurs at Ant. 2, resulting in poor isolation between the elements, as shown in Fig. 9. To address this issue, two metal vias are added along the symmetry axis, with their optimized size and position provided in Fig. 8(a). By introducing electric field nulls using the metal vias between the metal shell and the motherboard, the mode symmetry is disrupted and the mutual coupling is effectively reduced. As depicted in Fig. 9(a), the addition of the metal vias improves the isolation by up to 5.5 dB, while the S_{11} bandwidth remains almost unchanged. Over a wide bandwidth from 3.27 to 8.46 GHz, the MIMO antenna achieves an isolation greater than 12 dB, demonstrating its suitability for MIMO applications in metal-shell tablet computers.

To further illustrate the method for improving isolation, Fig. 10 shows the impact of the metal via position on antenna isolation. As seen, due to the periodic distribution of electric field amplitude in the cavity modes, the position of the vias significantly influences the antenna's isolation. By optimizing the via positions, enhanced isolation is achieved with just two vias. Additionally, increasing the number of vias can further improve the isolation, though it also increases the cost and complexity in engineering.

To demonstrate the practicality of our design, the proposed antenna is placed in a real tablet model for simulation. As shown in Fig. 11, the model consists of a mainboard (ground), a metal shell, and several internal components.

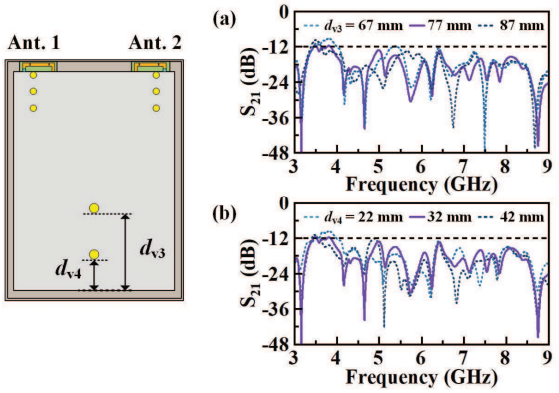

Fig. 10. Analyses of different parameters of the isolation metal vias. (a) d_{v3}. (b) d_{v4}.

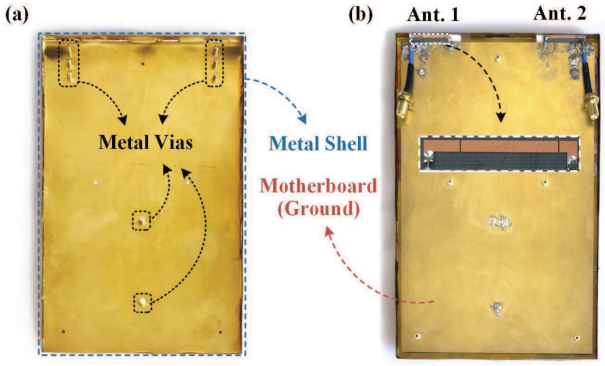

Fig. 12. Top view of the fabricated two-element MIMO antenna in the mock-up metal-shell tablet computer. (a) Internal and (b) external structures.

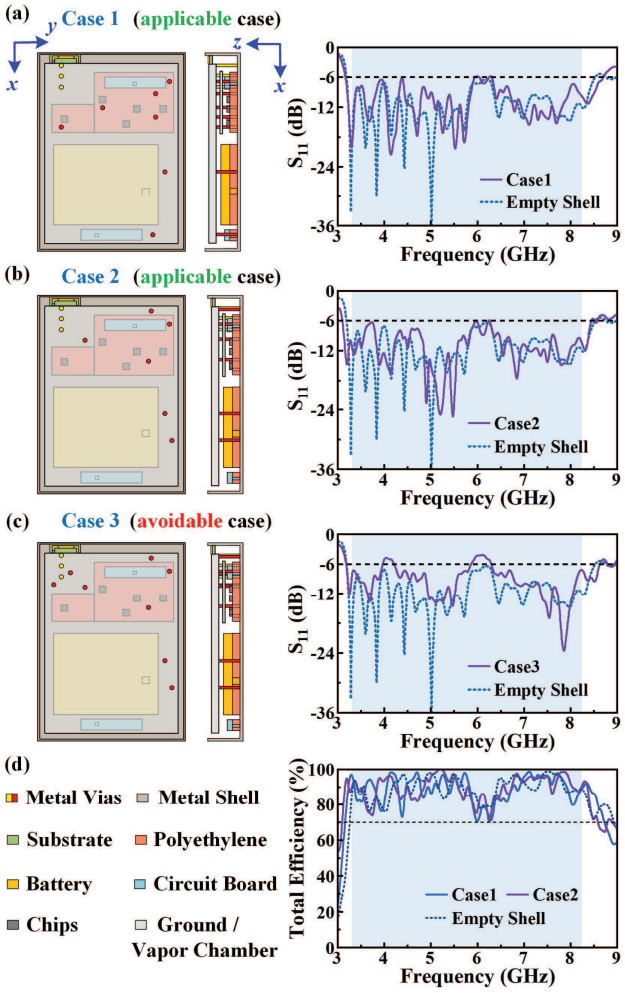

Fig. 11. Simulated antenna parameters in the real tablet model. Reflection coefficients in (a) Case 1, (b) Case 2, and (c) Case 3. (d) Total efficiency in Cases 1 and 2. (The red vias represent the newly added metal vias in the real tablet model.)

The nonmetallic components include an F4B substrate and polyethylene-based supporting structures, while the metallic components include a battery, chips, and circuit boards. Additionally, a vapor chamber (VC) structure is positioned above the circuit board to enhance the heat dissipation and electromagnetic shielding performance. Based on this model, Cases 1 and 2 illustrate two applicable via configurations commonly used in commercial tablets. As shown in Fig. 11(a) and (b), the electric field nulls introduced by the vias do not significantly affect impedance matching, owing to the excitation of higher order cavity modes. Additionally, in Case 3 of Fig. 11(c), when two additional vias are randomly placed near the antenna, wideband matching is severely degraded. However, in practical engineering, the positions of metal vias near the antenna can be flexibly optimized, making such adverse cases avoidable. Furthermore, Fig. 11(d) presents the total efficiencies for the two applicable cases. As observed, the total efficiency remains above 70% across the operating frequency range, meeting engineering requirements. In future work, we plan to incorporate structures such as conductive tapes and foams into the tablet environment to enhance thermal management and assembly reliability. These measures will further align the antenna's operating conditions with practical engineering scenarios. Overall, the proposed antenna demonstrates wide bandwidth and high efficiency within a real tablet environment, confirming its potential for practical applications.

III. Fabrication and Measurement

A prototype of the proposed two-element MIMO antenna embedded in a mock-up tablet computer was fabricated and measured to validate the antenna design method. Fig. 12 shows a photograph of the fabricated antenna and its tablet computer environment. As shown, the metal shell is constructed from a folded copper plate, with eight metal vias soldered to its bottom and simultaneously soldered to the motherboard (ground) above. Five M2-type plastic screws are utilized to ensure structural stability. The two symmetrical antenna elements, printed on F4B substrates, are positioned at the two upper corners of the mock-up tablet computer. Each antenna element is soldered to the motherboard at one end and fed by a 50-Ω semi-flexible coaxial cable, whose inner conductor is soldered to the other end of the antenna and outer conductor is soldered to the motherboard. The fabricated antenna was measured with an N9917A vector network analyzer for S-parameters and a standard microwave anechoic chamber for radiation properties.

The simulated and measured S-parameters of the proposed two-element MIMO antenna are presented in Fig. 13. As

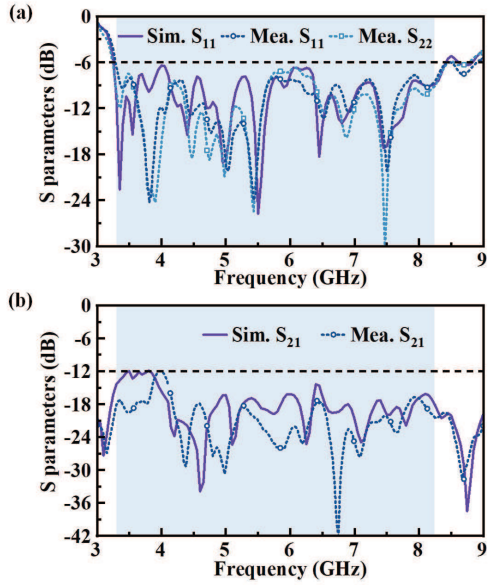

Fig. 13. Simulated and measured S-parameters of the proposed two-element MIMO antenna. (a) Reflection coefficients. (b) Transmission coefficients.

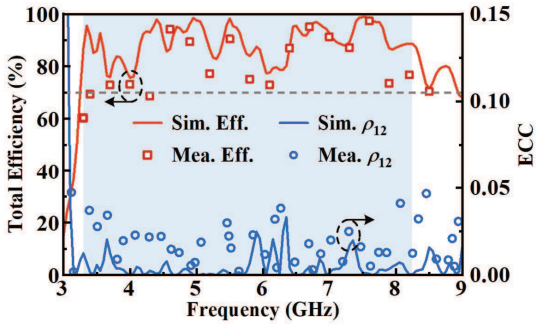

Fig. 14. Total efficiencies and ECC of the proposed MIMO antenna in simulated and measured results.

shown in Fig. 13(a), the measured reflection coefficients of both antenna elements exhibit a wide −6-dB impedance bandwidth of 3.27–8.46 GHz, covering multiple wireless communication bands, including 5G N77/N78/N79, Wi-Fi 6/6 E, and UWB channels 2–9. Meanwhile, the simulated and measured transmission coefficients, presented in Fig. 13(b), indicate an isolation of over 12 dB between the antenna elements across the entire operating bandwidth. Despite manufacturing errors and dielectric losses, the measured results closely align with the simulated ones. Furthermore, based on the simulated and measured S-parameters, the envelope correlation coefficient (ECC) between the two antenna elements is calculated and shown in Fig. 14. Across the entire operating frequency band, ρ_{12} remains below 0.05, satisfying the requirements for MIMO applications in practical engineering.

The simulated and measured total efficiencies are depicted as the red curve and points in Fig. 14, respectively. Due to the structural symmetry, only the results for Ant. 1 are presented. Within the operating bands, the simulated total efficiencies range from 75.7% to 98.2%, while the measured efficiencies vary from 68.7% to 97.3%. Since the antenna

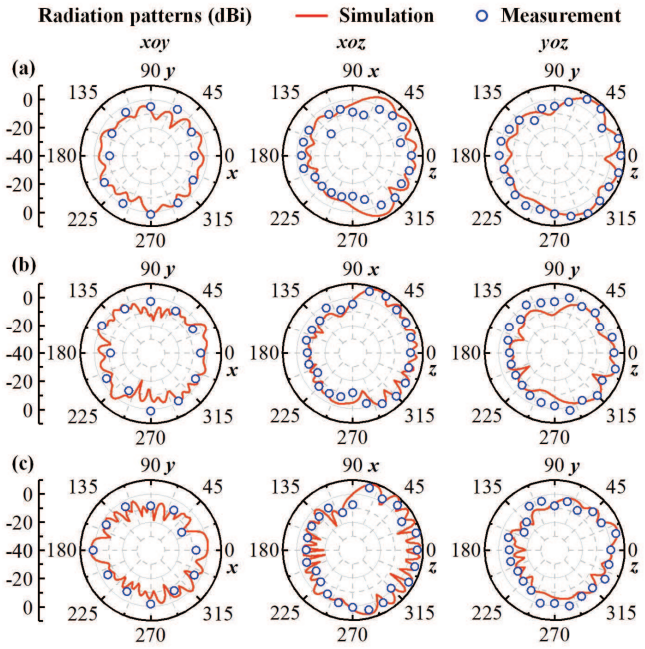

Fig. 15. Simulated and measured 2-D radiation patterns of Ant. 1 at (a) 4.4, (b) 7.6, and (c) 8.5 GHz.

primarily radiates through the metallic cavity, the total loss mainly originates from the return loss. The observed reduction in measured efficiency at certain frequency points is attributed to losses in the substrate and coaxial cable. Nonetheless, the efficiency meets the requirements for engineering applications. Fig. 15 presents the 2-D radiation patterns of Ant. 1 in different section planes. The measured results align well with the simulated ones across three coordinate planes. Besides, the antenna's radiation pattern exhibits no significant nulls throughout the entire space, which is beneficial for the stability of wireless communication in mobile terminals.

In previous work [22], a similar MNZ loop antenna is proposed to achieve broadband performance in a metal-shell tablet computer. However, this work does not fully explore the impact of the metal shell, limiting its utilization of the cavity modes induced between the metal shell and the motherboard. In contrast, our design achieves size miniaturization through the MNZ half-loop design and further enhances the antenna's bandwidth by effectively exciting and controlling multiple cavity modes. As a result, compared to the antenna proposed in [22], our design achieves a bandwidth improvement from 50% to 88.5% while maintaining a smaller size, making it better suited for broadband mobile communication applications.

To further highlight the advantages of our proposed antenna, Table II compares its performance with other wideband antennas designed for metal-shell terminals. The inverted-F antenna (IFA) [18] and half-loop antenna [19] achieve multifrequency performance through different matching circuits. However, their bandwidth-to-volume ratios (BVRs) are relatively low due to the bandwidth limitations of the circuit networks. The MNZ loop in [22] utilizes a balanced structure to mitigate the effects of the metal shell, thereby achieving higher efficiency, while it requires a larger space for wideband coverage. By

TABLE II
COMPARISON OF THE PROPOSED ANTENNA WITH OTHER WIDEBAND ANTENNAS IN METAL-SHELL TERMINALS

Ref.	Antenna type	Metal shell integrity	Element dimensions* (λ_L^3)	-6 dB Bandwidth	BVR ($\times 10^2$ λ_L^{-3})	Efficiency
[18]	IFA with matching network	No	0.13 × 0.021 × 0.036	1.56-1.58 GHz (1.3%) 2.40-2.48 GHz (3.3%) 5.15-5.88 GHz (13.2%)	1.32 3.36 13.43	>55%
[19]	Half loop with matching network	No	0.20 × 0.070 × 0.018	0.75-0.96 GHz (24.6%) 1.71-2.69 GHz (44.5%)	9.76 17.66	> 45%
[22]	Balanced MNZ Loop	Yes	0.67 × 0.099 × 0.015	4.5-7.5 GHz (50.0%)	5.03	> 70%
[25]	Open Slot	No	0.15 × 0.020 × 0.077	3.3-5.0 GHz (41.0%)	17.75	> 52.5%
[26]	Open Slot	No	0.17 × 0.044 × 0.055	3.3-7.2 GHz (74.3%)	18.05	> 40.5%
[27]	Open Slot	No	0.17 × 0.033 × 0.066	3.3-6.0 GHz (58.1%)	15.69	> 40%
[28]	Open Slot	No	0.20 × 0.009 × 0.079	3.4-6.1 GHz (56.8%)	39.94	> 58%
[29]	Open Slot	No	0.09 × 0.020 × 0.070	3.0-6.0 GHz (66.7%)	52.94	> 50%
Pro.	**MNZ Half Loop**	**Yes**	**0.28 × 0.047 × 0.011**	**3.27-8.46 GHz (88.5%)**	**61.14**	**> 68.7%**

*: Element dimensions are written in the order of length × clearance × height.
λ_L: Free-space wavelength at the lowest frequency in the band.
BVR: Bandwidth-to-volume ratio, which is calculated by dividing the fractional bandwidth by the electrical volume.

decoupling the back-to-back antenna pair, antennas in [25] and [26] achieve high isolation in a more compact size across a wide bandwidth. Antennas in [27], [28], and [29] achieve broadband performance in small dimensions, though their reduced efficiencies restrict their practicality. Furthermore, the antennas utilized in [18], [19], [25], [26], [27], [28], and [29] compromise the integrity of the metal shell, limiting their applications in engineering. In our design, through the effective excitation of multiple cavity modes, the proposed antenna achieves a wider bandwidth and a larger BVR without compromising the metal-shell structure. With the merits of broad bandwidth, compact size, and practical applicability, our proposed approach demonstrates significant advantages for antenna designs in metal-shell mobile terminals.

IV. CONCLUSION

In this article, we investigate the metal-shell effect on multimode antennas in mobile terminals and propose an alternative approach for bandwidth enhancement leveraging the metal shell. A design example of an MNZ half-loop antenna is presented and embedded in a mock-up tablet computer. The half-loop antenna, operating at its loop—0^{th}, 1^{st}, and 2^{nd} modes, contributes to couple the cavity—$TM_{8,2}$, $TM_{9,2}$, and $TM_{10,2}$ modes induced between the metal shell and the motherboard. The excitation of these cavity modes successfully enhances the antenna's bandwidth. Furthermore, a two-element MIMO antenna is constructed, with eight metal shorting vias employed to improve impedance matching and isolation. This design example, with antenna element dimensions of $0.28 \times 0.047 \times 0.011$ λ_L^3, achieves a wide bandwidth from 3.27 to 8.46 GHz and total efficiencies exceeding 68.7%. The isolation between the antenna elements is greater than 12 dB, and the ECC remains below 0.05. The measured results highlight the effectiveness of the proposed approach for designing compact, wideband antennas in metal-shell mobile terminals.

REFERENCES

[1] H. H. Park, "Reduction of electromagnetic noise coupling to antennas in metal-framed smartphones using ferrite sheets and multi-via EBG structures," *IEEE Trans. Electromagn. Compat.*, vol. 60, no. 2, pp. 394–401, Apr. 2018.
[2] D. Huang and Z. Du, "Eight-band antenna with a small ground clearance for LTE metal-frame mobile phone applications," *IEEE Antennas Wireless Propag. Lett.*, vol. 17, pp. 34–37, 2018.
[3] J. Bang and J. Choi, "A SAR reduced mm-wave beam-steerable array antenna with dual-mode operation for fully metal-covered 5G cellular handsets," *IEEE Antennas Wireless Propag. Lett.*, vol. 17, pp. 1118–1122, 2018.
[4] Y. Li, Z. Zhang, Z. Li, J. Zheng, and Z. Feng, "High-permittivity substrate multiresonant antenna inside metallic cover of laptop computer," *IEEE Antennas Wireless Propag. Lett.*, vol. 10, pp. 1092–1095, 2011.
[5] C. Deng, Z. Feng, and S. V. Hum, "MIMO mobile handset antenna merging characteristic modes for increased bandwidth," *IEEE Trans. Antennas Propag.*, vol. 64, no. 7, pp. 2660–2667, Jul. 2016.
[6] K. Li, Y. Zhang, and Y. Li, "Hepta-mode terminal microstrip antenna for mobile Wi-Fi 6/6E and UWB channels 5–11 MIMO applications," *IEEE Trans. Antennas Propag.*, vol. 72, no. 9, pp. 7048–7056, Sep. 2024.
[7] S. Wang and Y. Li, "Single-transistor impedance matching circuit for over-hundred-octave active antennas," *IEEE Trans. Antennas Propag.*, vol. 72, no. 3, pp. 2391–2398, Mar. 2024.
[8] S. Wang et al., "Antenna thousandfold miniaturization with ohmic-biased transistor circuit," *Electromag. sci.*, vol. 3, no. 2, pp. 1–12, Jun. 2025.
[9] Y. Zhang and Y. Li, "Wideband microstrip antenna in small volume without using fundamental mode," *Electromagn. Sci.*, vol. 1, no. 2, pp. 1–6, Jun. 2023.

[10] Y. Wang, L. Sun, Z. Du, and Z. Zhang, "Review antenna design for modern mobile phones: A review," *Electromagn. Sci.*, vol. 2, no. 2, pp. 1–36, Jun. 2024.
[11] Y. Zhang, Y. Li, W. Zhang, Z. Zhang, and Z. Feng, "Omnidirectional antenna diversity system for high-speed onboard communication," *Engineering*, vol. 11, pp. 72–79, Apr. 2022.
[12] L. Chang, H. Wang, Z. Zhang, Y. Li, and Z. Feng, "A dual-environment active RFID tag antenna mountable on metallic objects," *IEEE Antennas Wireless Propag. Lett.*, vol. 15, pp. 1759–1762, 2016.
[13] J.-H. Chou, J.-F. Chang, D.-B. Lin, H.-J. Li, and T.-L. Wu, "A compact loop-slot mode combination antenna for ultra-thin tablet computer with metallic bottom cover," *IEEE Antennas Wireless Propag. Lett.*, vol. 13, pp. 746–749, 2014.
[14] S.-C. Chen, C.-C. Huang, and W.-S. Cai, "Integration of a low-profile, long-term evolution/wireless wide area network monopole antenna into the metal frame of tablet computers," *IEEE Trans. Antennas Propag.*, vol. 65, no. 7, pp. 3726–3731, Jul. 2017.
[15] K.-L. Wong and C.-Y. Huang, "Triple-wideband open-slot antenna for the LTE metal-framed tablet device," *IEEE Trans. Antennas Propag.*, vol. 63, no. 12, pp. 5966–5971, Dec. 2015.
[16] H. Chen and A. Zhao, "LTE antenna design for mobile phone with metal frame," *IEEE Antennas Wireless Propag. Lett.*, vol. 15, pp. 1462–1465, 2016.
[17] K.-L. Wong and C.-Y. Tsai, "IFA-based metal-frame antenna without ground clearance for the LTE/WWAN operation in the metal-casing tablet computer," *IEEE Trans. Antennas Propag.*, vol. 64, no. 1, pp. 53–60, Jan. 2016.
[18] C.-Y. Tsai and K.-L. Wong, "Inverted-F antenna-based on-frame GPS/WLAN antenna for the metal-casing tablet computer," in *Proc. 10th Eur. Conf. Antennas Propag. (EuCAP)*, Apr. 2016, pp. 1–4.
[19] K.-L. Wong and C.-Y. Tsai, "Half-loop frame antenna for the LTE metal-casing tablet device," *IEEE Trans. Antennas Propag.*, vol. 65, no. 1, pp. 71–81, Jan. 2017.
[20] P. Yang, K. Yan, F. Yangl, L. Y. Zeng, and S. Huang, "Reconfigurable slot antenna design for 5G smartphone with metal casing," in *Proc. IEEE Int. Symp. Antennas Propag. USNC/URSI Nat. Radio Sci. Meeting*, Jul. 2018, pp. 453–454.
[21] M. Stanley, Y. Huang, H. Wang, H. Zhou, Z. Tian, and Q. Xu, "A novel reconfigurable metal rim integrated open slot antenna for octa-band smartphone applications," *IEEE Trans. Antennas Propag.*, vol. 65, no. 7, pp. 3352–3363, Jul. 2017.
[22] W. Yan et al., "Multimode balanced mu-near-zero loop antenna for Wi-Fi 6/6E applications in full metal housing tablet computers," *IEEE Trans. Antennas Propag.*, vol. 72, no. 7, pp. 5469–5478, Jul. 2024.
[23] K. Li et al., "Hybrid-loop antenna for dual-band Wi-Fi applications in mobile tablet computers," in *Proc. IEEE Int. Symp. Antennas Propag. INC/USNC-URSI Radio Sci. Meeting (AP-S/INC-USNC-URSI)*, Jul. 2024, pp. 2217–2218.
[24] L. Sun, Y. Li, Z. Zhang, and Z. Feng, "Wideband 5G MIMO antenna with integrated orthogonal-mode dual-antenna pairs for metal-rimmed smartphones," *IEEE Trans. Antennas Propag.*, vol. 68, no. 4, pp. 2494–2503, Apr. 2020.
[25] L. Sun, Y. Li, and Z. Zhang, "Wideband decoupling of integrated slot antenna pairs for 5G smartphones," *IEEE Trans. Antennas Propag.*, vol. 69, no. 4, pp. 2386–2391, Apr. 2021.
[26] L. Sun, Y. Li, and Z. Zhang, "Wideband integrated quad-element MIMO antennas based on complementary antenna pairs for 5G smartphones," *IEEE Trans. Antennas Propag.*, vol. 69, no. 8, pp. 4466–4474, Aug. 2021.
[27] X. Zhang, Y. Li, W. Wang, and W. Shen, "Ultra-wideband 8-port MIMO antenna array for 5G metal-frame smartphones," *IEEE Access*, vol. 7, pp. 72273–72282, 2019.
[28] H. Varheenmaa, P. Ylä-Oijala, A. Lehtovuori, and V. Viikari, "Wideband sub-6 GHz MIMO antenna for full-screen metal rim smartphones," *IEEE Access*, vol. 11, pp. 111888–111896, 2023.
[29] H.-D. Chen, Y.-C. Tsai, C.-Y.-D. Sim, and C. Kuo, "Broadband eight-antenna array design for sub-6 GHz 5G NR bands metal-frame smartphone applications," *IEEE Antennas Wireless Propag. Lett.*, vol. 19, pp. 1078–1082, 2020.
[30] K. Wei, Z. Zhang, Z. Feng, and M. F. Iskander, "A MNG-TL loop antenna array with horizontally polarized omnidirectional patterns," *IEEE Trans. Antennas Propag.*, vol. 60, no. 6, pp. 2702–2710, Jun. 2012.
[31] K. Wei, Z. Zhang, and Z. Feng, "Design of a wideband horizontally polarized omnidirectional printed loop antenna," *IEEE Antennas Wireless Propag. Lett.*, vol. 11, pp. 49–52, 2012.
[32] K. Wei, Z. Zhang, Z. Feng, and M. F. Iskander, "A wideband MNG-TL dipole antenna with stable radiation patterns," *IEEE Trans. Antennas Propag.*, vol. 61, no. 5, pp. 2418–2424, May 2013.
[33] H. Li and Y. Li, "Mode compression method for wideband dipole antenna by dual-point capacitive loadings," *IEEE Trans. Antennas Propag.*, vol. 68, no. 8, pp. 6424–6428, Aug. 2020.
[34] H. Li, Z. Zhou, Y. Zhao, and Y. Li, "Low-loss beam synthesizing network based on Epsilon-near-zero (ENZ) medium for on-chip antenna array," *Chip*, vol. 2, no. 2, Jun. 2023, Art. no. 100049.
[35] Z. Zhou et al., "Dispersion coding of ENZ media via multiple photonic dopants," *Light, Sci. Appl.*, vol. 11, no. 1, Jul. 2022, Art. no. 207.

Kaifeng Li received the B.S. degree in electronic engineering from Tsinghua University, Beijing, China, in 2024, where he is currently pursuing the Ph.D. degree in electronic engineering.

His current research interests include wideband antennas, terminal antennas, and metamaterial antennas.

Wendi Yan (Graduate Student Member, IEEE) received the B.S. degree in electronic engineering from Tsinghua University, Beijing, China, in 2021, where he is currently pursuing the Ph.D. degree in electronic engineering.

His current research interests include terminal antennas, metamaterial antennas, epsilon-near-zero antennas, and mu-near-zero antennas.

Yongjian Zhang (Member, IEEE) received the B.S. degree in communication engineering from Tongji University, Shanghai, China, in 2018, and the Ph.D. degree in electronic engineering from Tsinghua University, Beijing, China, in 2023.

He is currently a Post-Doctoral Fellow with the Department of Electronic Engineering, Tsinghua University. His current research interests include aircraft antennas, dual-polarized antennas, and multiple-input–multiple-output (MIMO) antenna arrays.

Dr. Zhang serves as a reviewer for IEEE TRANSACTIONS ON ANTENNAS AND PROPAGATION, IEEE ANTENNAS AND WIRELESS PROPAGATION LETTERS, and *Microwave and Optical Technology Letters*.

Peihang Li received the B.S. degree from Shanxi University, Taiyuan, China, in 2020, and the M.S. degree from the University of Electronic Science and Technology of China, Chengdu, China, in 2023. He is currently pursuing the Ph.D. degree in electronic engineering with Tsinghua University, Beijing, China.

His current research interests include terminal antennas, metamaterial antennas, and epsilon-near-zero antennas.

Pengyu Fu received the B.S. degree and the Ph.D. degree in electronic engineering from Tsinghua University, Beijing, China, in 2021 and 2025, respectively.

He is currently a Post-Doctoral Fellow with the Department of Electronic Engineering, Tsinghua University. His current research interests include metamaterials and metamaterial-inspired antennas.

Dr. Fu serves as a reviewer for *Microwave and Optical Technology Letters*.

Yixiang Song received the B.S. degree in applied physics from Hefei University of Technology, Hefei, Anhui, China, in 1997.

He is currently with Lenovo Group, Beijing, China. His research interests include terminal antennas, RF technology, and tablet wireless systems.

Hui Lin received the B.S. and M.S. degrees from the University of Science and Technology of China, Hefei, China, in 2003 and 2006, respectively.

He is currently with Lenovo Group, Shanghai, China. His research interests include antennas, RF components, and tablet hardware systems.

Heng Guo received the B.S. and M.S. degrees in electronic and information engineering from Beihang University, Beijing, China, in 2006 and 2009, respectively.

He is currently with Lenovo Group, Beijing. His research interests include small antennas, circularly polarized antennas, and smart antennas.

Shumin Liao received the B.E. degree from Hubei Normal University, Huangshi, Hubei, China, in 2017, and the M.S. degree in information and communication engineering from Shenzhen University, Shenzhen, China, in 2020.

She is currently an Antenna Engineer with the Department of Tablet Business, Lenovo Group Ltd., Beijing, China. Her current research interests include the development and application of mobile terminal antennas.

Yue Li (Senior Member, IEEE) received the B.S. degree in telecommunication engineering from Zhejiang University, Zhejiang, China, in 2007, and the Ph.D. degree in electronic engineering from Tsinghua University, Beijing, China, in 2012.

In June 2012, he was a Post-Doctoral Fellow with the Department of Electronic Engineering, Tsinghua University. In December 2013, he was a Research Scholar with the Department of Electrical and Systems Engineering, University of Pennsylvania, Philadelphia, PA, USA. He was also a Visiting Scholar with the Institute for Infocomm Research (I2R), A*STAR, Singapore, in 2010, and Hawaii Center of Advanced Communication (HCAC), University of Hawaii at Manoa, Honolulu, HI, USA, in 2012. Since January 2016, he has been with Tsinghua University, where he is currently an Assistant Professor. He is an Associate Professor with the Department of Electronic Engineering, Tsinghua University. He has authored and co-authored over 260 journal articles and 50 international conference papers and holds 25 granted Chinese patents. His current research interests include metamaterials, plasmonics, electromagnetics, nanocircuits, mobile and handset antennas, MIMO and diversity antennas, and millimeter-wave antennas and arrays.

Dr. Li was a recipient of the Issac Koga Gold Medal from the URSI General Assembly. He served as an Associate Editor for IEEE TRANSACTIONS ON ANTENNAS AND PROPAGATION andIEEE ANTENNAS AND WIRELESS PROPAGATION LETTERS from 2017 to 2024. He is also serving as an Associate Editor for *Microwave and Optical Technology Letters* and *Computer Applications in Engineering Education*.